Three-dimensional visualization of choroidal vessels by using standard and ultra-high resolution scattering optical coherence angiography

Youngjoo Hong[1, 2*], Shuichi Makita[1], Masahiro Yamanari[1], Masahiro Miura[1,3], Soohyun Kim[2], Toyohiko Yatagai[1], and Yoshiaki Yasuno[1]**

[1]*Computational Optics Group in University of Tsukuba, Tennodai, Tsukuba, Ibaraki 305-8573, Japan and Computational Optics and Ophthalmology Group, Tsukuba, Ibaraki, 305-8573, Japan*
[2] *Department of Mechanical Engineering, KAIST, Guseong-dong, Yuseong, Daejeon 305-701, Republic of Korea*
[3]*Department of Ophthalmology, Tokyo Medical University, Shinjuku, Tokyo, Japan*
* hongyoungjoo@kaist.ac.kr; ** yasuno@optlab2.bk.tsukuba.ac.jp
http://optics.bk.tsukuba.ac.jp/COG/

Abstract: Scattering optical coherence angiography (S-OCA) is a non-invasive imaging method that is based on the high-speed standard 800nm band spectral-domain optical coherence tomography (SD-OCT) and the ultra-high-resolution SD-OCT which has the axial resolution of 6.1 μm and 2.9 μm in tissue, respectively. In this paper, we have demonstrated the use of this method for *in vivo* human retinal imaging. A three-dimensional view of the choroidal vasculature was obtained by segmenting the choroidal vessels; this was done using intensity threshold based binarization at each depth plane relative to the retinal pigment epithelium. A vascular projection image was obtained by integrating the segmented choroidal vasculature. In order to assess the feasibility of the proposed method, we compared these images with those obtained using existing invasive methods such as fluorescein angiography and indocyanine green angiography. Clinically worthful images are obtained from the application of S-OCA to the age-related macular degeneration and polypoidal choroidal vasculopathy.

OCIS codes: (170.4470) Ophthalmology; (170.4500) Optical coherence tomography; (100.6890) Three-dimensional image processing; (110.4500) Optical coherence tomography.

References and links

1. J. Flammer, S. Orgul, V. P. Costa, N. Orzalesi, G. K. Krieglstein, L. M. Serra, J.-P. Renard, and E. Stefansson," The impact of ocular blood flow in glaucoma," Prog. Retin. Eye Res. **21**, 359−393 (2002).
2. V. Patel, S. Rassam, R. Newsom, J. Wiek, and E. Kohner, "Retinal blood flow in diabetic retinopathy," BMJ **305**, 678–683 (1992).
3. E. Friedman, "A hemodynamic model of the pathogenesis of age-related macular degeneration," Am. J. Ophthalmol. **124**, 677–682 (1997).
4. J. D. Gass, *Stereoscopic atlas of macular diseases*, 4th ed., (Mosby, 1997).
5. K. A. Kwiterovich, M. G. Maguire, R. P. Murphy, A. P. Schachat, N. M. Bressler, S. B. Bressler, and S. L. Fine, "Frequency of adverse systemic reactions after fluorescein angiography. Results of a prospective stud," Ophthalmology **98**, 1139−1142 (1991).
6. M. Hope-Ross, L. Yannuzzi, E. Gragoudas, D. Guyer, J. Slakter, J. Sorenson, S. Krupsky, D. Orlock, and C. Puliafito, "Adverse reactions due to indocyanine green," Ophthalmology **101**, 529-533 (1994).
7. D. Huang, E. A. Swanson, W. G. S. C. P. Lin, J. S. Schuman, W. Chang, T. F. M. R. Hee, K. Gregory, C. A. Puliafito, and J. G. Fujimoto, "Optical coherence tomography," Science **254**, 1178–1181 (1991).
8. A. F. Fercher, C. K. Hitzenberger, G. Kamp, and S. Y. El-Zaiat, "Measurement of intraocular distances by backscattering spectral interferometry," Opt. Commun. **117**, 43–48 (1995).
9. G. Häusler and M. W. Lindner, "Coherence rader" and "spectral radar" —New tools for dermatological diagnosis," J. Biomed. Opt. **3**, 21-31 (1998).
10. Y. Zhao, Z. Chen, C. Saxer, S. Xiang, J. F. de Boer, and J. S. Nelson, "Phase-resolved optical coherence tomography and optical Doppler tomography for imaging blood flow in human skin with fast scanning speed and high velocity sensitivity," Opt. Lett. **25**, 114-116 (2000).

#80285 - $15.00 USD Received 22 Feb 2007; revised 2 May 2007; accepted 3 May 2007; published 5 Jun 2007

11. R. A. Leitgeb, C. K. Hitzenberger, A. F. Fercher, and T. Bajraszewski, "Phase-shifting algorithm to achieve high-speed long-depth-range probing by frequency-domain optical coherence tomography," Opt. Lett. **28**, 2201-2203 (2003).
12. R. Leitgeb, L. F. Schmetterer, M. Wojtkowski, C. K. Hitzenberger, M. Sticker, andd A. F. Fercher, "Flow velocity measurements by frequency domain short coherence interferometry," Proc. SPIE **4619,** 16-21 (2002).
13. B. R. White, M. C. Pierce, N. A. Nassif, B. Cense, B. H. Park, G. J. Tearney, B. E. Bouma, T. C. Chen, and J. F. de Boer, "In vivo dynamic human retinal blood flow imaging using ultra-high-speed spectral domain optical Doppler tomography," Opt. Express **11**, 3490 (2003).
14. S. Yazdanfar, A. M. Rollins, and J. A. Izatt, "In vivo imaging of human retinal flow dynamics by color Doppler optical coherence tomography," Arch. Ophthalmol. **121**, 235–239 (2003).
15. S. Makita, Y. J. Hong, M. Yamanari, T. Yatagai, and Y. Yasuno, "Optical coherence angiography," Opt. Express **14**, 7821-7840 (2006).
16. B. Povazay, K. Bizheva, B. Hermann, A. Unterhuber, H. Sattman, A. F. Fercher, W. Drexler, C. Schubert, P. K. Ahnelt, M. Mei, R. Holzwarth, W. J. Wadsworth, J. C. Knight, and P. S. Russel, "Enhanced visualization of choroidal vessels using ultrahigh resolution ophthalmic OCT at 1050 nm," Opt. Express **11,** 1980-1986 (2003).
17. A. Unterhuber, B. Povazay, B. Hermann, H. Sattmann, A. Chavez-Pirson, and W. Drexler, "In vivo retinal optical coherence tomography at 1040 nm - enhanced penetration into the choroids," Opt. Express **13**, 3252-3258 (2005).
18. E. C. W. Lee, J. F. de Boer, M. Mujat, H. Lim, S. H. Yun, "In vivo optical frequency domain imaging of human retina and choroid," Opt. Express **14,** 4403-4411 (2006).
19. M. Hammer, A. Roggan, D. Schweitzer and G. Müller, "Optical properties of ocular fundus tissues-an in vitro study using the double-integrating-sphere technique and inverse Monte Carlo simulation," Phys. Med. Biol. **40**, 963-978 (1995).
20. A. Roggan, M. Friebel, K. Dörschel, A. Hahn, and G. Müller, "Optical properties of circulating human blood in the wavelength range 400–2500 nm," J. Biomed. Opt. **4**, 36–46 (1999).
21. Y. Yasuno, Y. J. Hong, S. Makita, M. Yamanari, M. Akiba, M. Miura, and T. Yatagai, "In vivo high-contrast imaging of deep posterior eye by 1-μm swept source optical coherence tomography and scattering optical coherence angiography," Opt. Express **15**, 6121-6139 (2007).
22. R. Leitgeb, W. Drexler, A. Unterhuber, B. Hermann, T. Bajraszewski, T. Le, A. Stingl, and A. Fercher, "Ultrahigh resolution Fourier domain optical coherence tomography," Opt. Express **12**, 2156-2165 (2004).
23. M. Wojtkowski, V. Srinivasan, T. Ko, J. Fujimoto, A. Kowalczyk, and J. Duker," Ultrahigh-resolution, high-speed, Fourier domain optical coherence tomography and methods for dispersion compensation," Opt. Express **12**, 2404-2422 (2004).
24. B. Cense, N. A. Nassif, T. C. Chen, M. C. Pierce, S. H. Yun, B. H. Park, B. E. Bouma, G. J. Tearney, and J. F. de Boer, "Ultrahigh-resolution high-speed retinal imaging using spectral-domain optical coherence tomography," Opt. Express **12**, 2435–2447 (2004).
25. American National Standards Institute, *American National Standard for Safe Use of Lasers: ANSI Z136.1* (Laser Institute of America, Orlando, Florida, 2000).
26. Y. Hori, Y. Yasuno, S. Sakai, M. Matsumoto, T. Sugawara, V. D. Madjarova, M. Yamanari, S. Makita, T. Yasui, T. Araki, M. Itoh, and T. Yatagai, "Automatic characterization and segmentation of human skin using three-dimensional optical coherence tomography," Opt. Express **14,** 1862-1877 (2006).
27. M. Mujat, R. C. Chan, B. Cense, B. H. Park, C. Joo, T. Akkin, T. C. Chen, and J. F. de Boer, "Retinal nerve fiber layer thickness map determined from optical coherence tomography images," Opt. Express **13,** 9480-9491 (2005).
28. S. Jiao, R. Knighton, X. Huang, G. Gregori, and C. A. Puliafito, "Simultaneous acquisition of sectional and fundus ophthalmic images with spectral-domain optical coherence tomography," Opt. Express **13**, 444-452 (2005).

1. Introduction

Examination of ocular vascular integrity is important for the diagnosis of ophthalmic diseases, because via the ocular vessels, the eye receives nourishment and wastes are removed. Glaucoma [1], diabetic retinopathy [2] and age-related macular degeneration (AMD) [3] are representative examples of ocular diseases. Among these, AMD is the leading cause of vision loss in America. One of the theoretical bases regarding AMD etiology is vascular degeneration. When the blood vessels have some problem to do their function, to compensate the malfunction of the blood vessels new abnormal blood vessels called choroidal neovascularization (CNV) are created. However, these blood vessels cause more problems. Fluorescein angiography (FA) and indocyanine green angiography (ICGA) are two commonly used methods to image ocular vessels [4]. With FA, which is a standard modality, retinal structure is satisfactorily visualized; however it is often difficult to visualize choroidal vasculature because of the short excitation wavelength (520 nm) of the sodium fluorescein dye.

#80285 - $15.00 USD Received 22 Feb 2007; revised 2 May 2007; accepted 3 May 2007; published 5 Jun 2007

In contrast, the choroidal vasculature is adequately visualized with ICGA because of the longer excitation wavelength (830 nm) of the indocyanine green (ICG) dye. In these two methods, the dye is injected into a vein in order to facilitate visualization of the blood vessels. The dye injection process is uncomfortable for patients, and some adverse allergic reactions may be induced [5, 6]. The sodium fluorescein dye used in FA can induce nausea, vomiting, itching, dyspnea and etc. Adverse allergic reactions are no longer common in ICGA; nonetheless this technique should be used with caution in individuals with a history of allergy to iodide and shellfish. Even though the choroidal vessels can be visualized on ICGA, it is occasionally difficult to resolve the tangled mass of vessels because they appear low in contrast and are overlapped by other choroidal vessels that lie in the background.

Optical coherence tomography (OCT) [7] is a noninvasive medical imaging method that is based on the principle of low-coherence interferometry, and it produces high resolution, cross-sectional images of biological tissues. High-resolution images can be rapidly obtained using the recently developed SD-OCT method [8, 9]. Additionally, blood flow velocity can be measured from the phase changes between adjacent A-lines, and the characteristic of flow dynamics of the blood vessels can be studied using Doppler OCT [10-14]. Makita *et al* demonstrated the use of Doppler optical coherence angiography (D-OCA) [15]. Three-dimensional (3D) images of the ocular vasculature were obtained wherein the retinal vessels were identified by observing the bidirectional flow of blood in them, and the choroidal vessels were identified by determining the power of Doppler shift. The retinal and choroidal regions were distinguished by the segmentation of the RPE. D-OCA facilitated reconstruction of the 3D vasculature based on the Doppler shift frequencies of the blood flow. Although D-OCA satisfied the requirement for the noninvasive measurement and 3D vasculature, but there is limitation of the measurable Doppler shift frequency. Therefore, it is difficult to detect the relatively low or high blood flow velocity. In D-OCA, dense scanning between the A-lines is necessary in order to measure the phase changes. However, dense scanning is expensive because it prolongs the measurement time, particularly in the case of 3D measurements, and some patients experience difficulty in enduring the extended measurement times and in avoiding eye movements during scanning.

With D-OCA, the choroidal vasculature is not as accurately imaged as the retinal vasculature. Cross-sectional choroidal vessels were clearly imaged by 1 μm band time-domain OCT by using the deep penetration property of this wavelength [16, 17], and 3D choroidal vessel structure were obtained by 1 μm SS-OCT that is also referred to optical frequency domain imaging (OFDI) [18]. Yasuno *et al.* applied a 3D segmentation of the choroidal vasculature; a scattering optical coherence angiography (S-OCA) method, which is based on the light absorption and the scattering properties of blood [19, 20], to the 3D OCT volume acquired by 1 μm SS-OCT [21]. S-OCA works well with this 1 μm band OCT. On the other hand, a 800 nm probe beam is commonly used for retinal OCT at this time, although the choroidal vessels have less contrast with this wavelength band. Hence it might be interesting and useful to apply the S-OCA method to 800 nm band OCT. This paper is the first demonstration of the application of the S-OCA method to 800 nm OCT, which has also been employed for the previously demonstrated D-OCA method [15]. The 3D images of the choroidal vasculature and the two-dimensional (2D) projection images obtained by this method were comparable with those obtained by D-OCA and were similar to the images obtained by ICGA. The S-OCA was then applied to the results of the UHR-SD-OCT [22-24]. This produced better image qualities of the segmented 3D choroidal vasculature and 2D projection angiograms, and UHR-S-OCA was more effective than the standard SD-OCT in revealing the finer structures of the vasculature. Although the lateral resolution was identical in both methods, the high axial resolution in the latter method is responsible for these improvements. For the clinical application, the eye measurement results of AMD patient with low-density scanning and PCV patient with high-density scanning were processed with S-OCA, and clinically meaningful images were obtained.

#80285 - $15.00 USD Received 22 Feb 2007; revised 2 May 2007; accepted 3 May 2007; published 5 Jun 2007

2. OCT Systems

In S-OCA, two OCT systems are employed to obtain intensity data of the retinal structure. One is the standard SD-OCT that was employed for the previously demonstrated D-OCA [15] and the other is UHR-SD-OCT. A broadband spectral light source (T870-HP, Superlum, Russia), which has a center wavelength of 870 nm and a full-width half-maximum (FWHM) spectral bandwidth of 170 nm, was employed in order to implement high axial resolution. An OCT proven broadband 2×2 fiber-optic coupler (Thorlab), which has an operating wavelength region of 850 ± 40 nm, was employed to split the beam; the distribution was 90% and 10% for the reference and sample arms, respectively. Fiber distortion polarization controllers were placed after the light source, and before the reference and sample arms of the OCT system. An optical isolator was used to prevent re-incident light back to the light source. A 78-D lens was employed to focus the probe beam on the posterior eye. The optical probing power at the sample position is 400 μW which is lower than the specified American National Standard Institute (ANSI) exposure limit [25]. The light backscattered from the retina and the reflected reference light from the mirror are combined and then guided to the spectrometer. A transparent diffraction grating (Wasatch Photonics, 1200 lines/mm) is employed to diffract the coherent light beam and an achromatic lens (f = 100 mm) is used to focus the diffracted light on a CCD camera. A high-speed line-scan CCD camera (Atmel, Aviiva M2CL), which has 2048 pixels of 14 μm square size is employed to detect the spectral interference signals.

This UHR-SD-OCT system is operated with an imaging performance of the 27 kHz A-line scan rate with a 36 μs exposure time for one A-line. A 2D B-scan image of 1024 A-lines was obtained at the rate of 26.4 frames/s, and a 3D volume of 1024 × 140 A-lines 3D volume was obtained in 5.5 s. The theoretical axial resolution was estimated to be 1.96 μm in air, but the experimental axial resolution in air was measured to be 4 μm. Assuming that the refractive index of the tissue is 1.38, this resolution value corresponds to 2.9 μm in the tissue. The experimental sensitivity of this system was measured to be 94 dB at a depth of 100 μm, while the theoretical sensitivity is 100.5 dB. These discrepancies in the experimental and theoretical values of the axial resolution and the sensitivity may be due to the insufficient use of the broadband spectral light source. Because of the dispersion of fiber optics, it is difficult to transmit the beam to the reference and sample arms with equal proportion through the whole wavelength region. Curvature of the image plane in the spectrometer also makes it difficult to focus whole of wavelength components to the line CCD sensor and from that curvature fringe contrast is worsen in the out of focus area. 3. Scattering optical coherence angiography

3. Scattering optical coherence angiography

S-OCA has been demonstrated by Yasuno *et al.* by using 1 μm SS-OCT, and the details of the algorithm has been described in Ref. 21. Here we briefly summarize the method. The basic principle of the S-OCA method is the segmentation of the choroidal vessels by using intensity threshold-based binarization (ITB). Although this principle is rather simple, because the signal decay varies depending on the depth, it is difficult to apply the ITB technique to the OCT images. In order to prevent this problem, we employ a method similar to that demonstrated by Hori *et al.* [26]; however, we specially modified this method for the purpose of the optical coherence angiography to segment three-dimensional choroidal vasculature.

The 3D OCT intensity volume of the retina is used to segment 3D choroidal vasculature. Three layers are segmented from the cross-sectional images of the 3D OCT volume, in order to identify the choroidal region. The first layer is the retinal surface, namely internal limiting membrane [27]. Another layer is a high-reflective layer that corresponds to the RPE complex; this complex comprises the inner/outer segment junction (IS/OS), RPE, and choriocapillary layer (CC). The other layer is the virtual posterior boundary of the choroid wherein the OCT signal balances to the noise level [21]. We defined the choroidal region as an area between RPE and the virtual posterior boundary.

After we segment out the choroid, the structure is realigned to the RPE. With this realignment, the intensity decay in the en-face plane at the same depth from the RPE is

#80285 - $15.00 USD Received 22 Feb 2007; revised 2 May 2007; accepted 3 May 2007; published 5 Jun 2007

assumed to be nearly even. The intensity distribution at each depth of the en-face plane is obtained and the pixels which suffice the following criteria are selected as the choroidal vessels;,

$$I_n < I'(x, y) < \mu - \sigma / 2 \tag{1}$$

where μ and σ are the mean intensity and the intensity standard deviation of the en-face image, respectively, and I_n is the noise level, and a binary mask is created for this vessel segmentation. The en-face intensity plane is multiplied with the binary mask and the selected intensity values are inverted and rescaled to the maximum intensity of the depth. This operation is iteratively processed at every depth, starting from the RPE to the posterior layer. 2D vascular masks of the segmented choroidal vasculature could thus be obtained for the entire depth. The RPE boundary position data is used to realign these 2D vascular masks to their original positions; this is done in order to obtain 3D images of the choroidal vasculature. A 3D Gaussian filter is applied for 3D volume rendering in order to suppress some noise particles. This procedure of the S-OCA algorithm is summarized in Fig. 1.

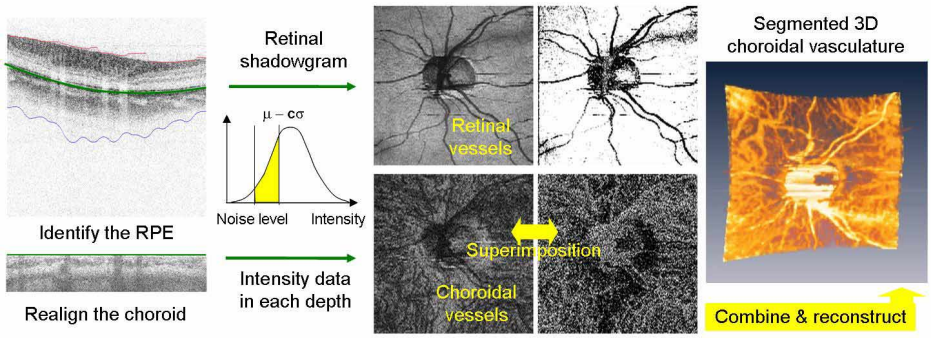

Fig. 1. Procedure of 3D choroidal vessel segmentation

4. Results and discussion

4.1 S-OCA using the Standard SD-OCT

Measurements were performed in a human eye devoid of any retinal diseases; the standard SD-OCT system was used for measurement, and the choroidal vessels were visualized *in vivo* 3D choroidal vasculatures were visualized by S-OCA according to the procedure described in section 3. Figure 2 and its movie represent the segmented choroidal vasculature of the macula and the optic nerve head (ONH) area that have a lateral size of 5 mm × 5 mm (1024 × 140 A-lines). Shadows of the retinal vessels were included in the 3D volume, that could make some confusion with choroidal vessels, but we could distinguish the shadow from the choroidal vessels with using a retinal shadowgram [28]. The 3D choroidal vascular networks can be observable.

#80285 - $15.00 USD Received 22 Feb 2007; revised 2 May 2007; accepted 3 May 2007; published 5 Jun 2007

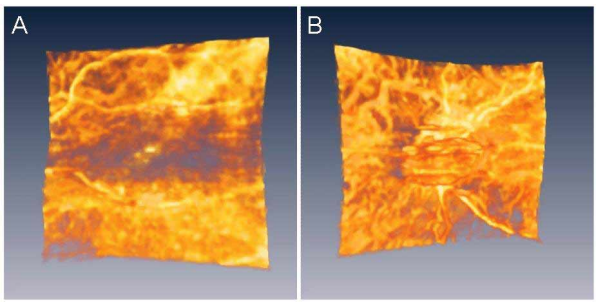

Fig. 2. 3D choroidal vascular images obtained using S-OCA; (A) is the macular area (1.35MB movie) and (B) is the ONH area (1.42 MB movie).

Figure 3 and Fig. 4 represent the en face projection images of the 3D S-OCA of the ONH and macula, respectively. A 2D retinal vessel image was obtained using a shadowgram [Fig. 3(A) and Fig. 4(A)] and a choroidal vessel image is the projection of the S-OCA [Fig. 3(B) and Fig. 4(B)]. For the contrast enhancement of the choroidal vessels in the projection image, we averaged a constant thickness of 284 μm approximately corresponding to the choroidal tissue region [14]. The two projection images were combined, and different color-maps were used to identify the each vessel; the retinal vessels and choroidal vessels are indicated in red and cyan, respectively [Fig. 3(C) and Fig. 4(C)].

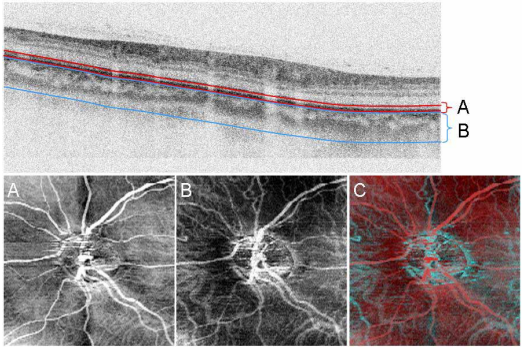

Fig. 3. 2D S-OCA of the ONH, (A) a shadowgram of the retinal vessels and (B) segmented choroidal vascular image are obtained by the projection in the RPE and choroidal regions, respectively. (C) is a combination of (A) and (B).

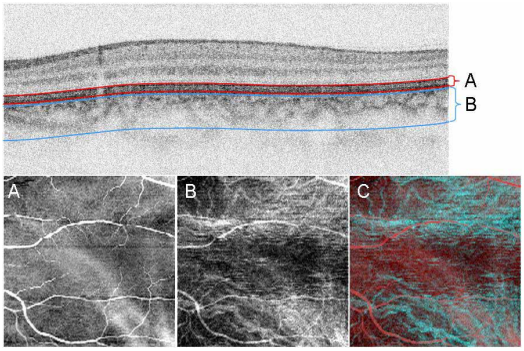

Fig. 4. 2D S-OCA of the macula, (A) a shadowgram of the retinal vessels and (B) segmented choroidal vascular image are obtained by the projection in the RPE and choroidal regions, respectively. (C) is a combination of (A) and (B).

#80285 - $15.00 USD Received 22 Feb 2007; revised 2 May 2007; accepted 3 May 2007; published 5 Jun 2007

4.2 Comparison of OCA and dye-injection angiographies

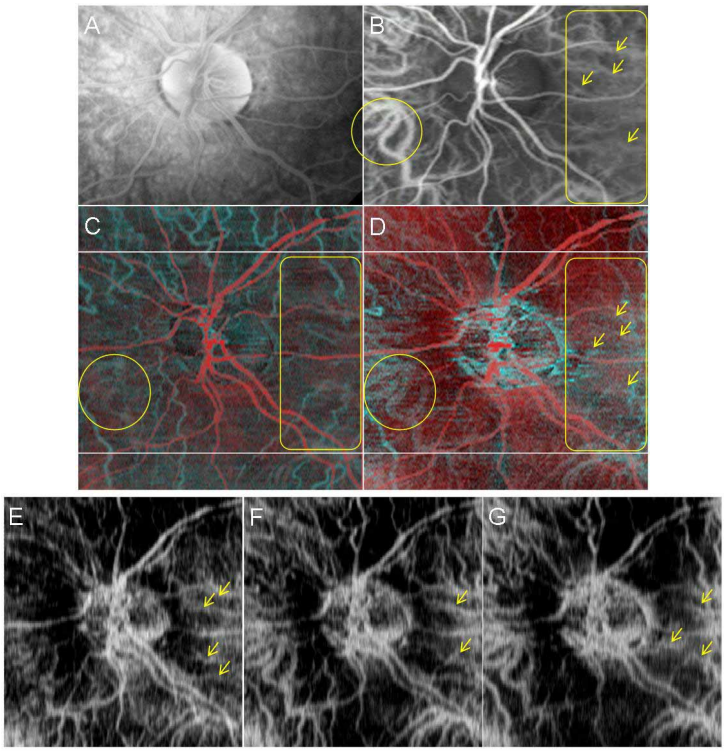

Fig. 5. Comparison of angiography images of the ONH; each image is obtained using (A) FA, (B) ICGA, (C) D-OCA and (D) S-OCA. Subsections (E), (F) and (G) represent sliced images of the segmented choroidal vasculature at different depths relative to the RPE, i.e., at 71, 107, and 142 μm, respectively (2.46MB movie).

An image of the ONH area obtained using S-OCA is compared with the FA, ICGA, and D-OCA images, as shown in Fig. 5 where Figs. 5(A) and 5(B) show FA and ICGA, respectively, while Figs. 5(C) and 5(D) show D-OCA and S-OCA. Since the area of the FA and ICGA images are smaller than those of OCA, the corresponding areas of the S-OCA and D-OCA images are cropped by lines. Some similarities can be observed in the images obtained using these four different techniques. In the D-OCA, the power of the Doppler shift signal is projected in the retinal and choroidal regions [15]. The retinal vessel images obtained using these four methods could be similar. However, the choroidal vessel images obtained using S-OCA and D-OCA differ slightly. Generally, the choroidal vessels appear clearer in D-OCA image than in S-OCA. However, some choroidal vessels that did not appear in the D-OCA image were visible in S-OCA. These differences can be noted in the area indicated by the yellow circle. The identical choroidal vessels are indicated in the yellow-circled area in Fig. 5(B) and Fig. 5(D); however, it is difficult to find these choroidal vessels in the same area in Fig. 5(C). Further, another difference can be noted in the central right portion of each angiogram that is indicated by a yellow rectangle. In Fig. 5(B), a few horizontally stretched choroidal vessels can be shown with low contrast. The similar faint choroidal vessels can be observed in the rectangular area in Fig. 5(D) as indicated by the yellow arrows.

#80285 - $15.00 USD Received 22 Feb 2007; revised 2 May 2007; accepted 3 May 2007; published 5 Jun 2007

S-OCA does not contrast the blood flow but segments the choroidal vessels by using OCT intensity; hence it is possible that low scattering non-vessel regions are selected as blood vessels in error. On the other hand, D-OCA discriminates the blood vessels by assessing their blood flow; however, this method requires high phase stability and it results in the relatively long acquisition time. These differences provide the different image properties and different applicability to these two OCA methods.

On performing intensity integration relative to the depth, the contrast of the tangled or densely gathered vessels decreases, because the intensity is averaged with that of the adjacent vessels. We can more easily resolve and recognize the each vessel within en-face slicing the segmented choroidal vasculature through the depth. Figs. 5(E), 5(F) and 5(G) represent the en-face sliced layer at a depth relative to the RPE, i.e, 71, 107, and 142 μm, respectively. We can attribute these image differences to the phase sensitivities of D-OCA and S-OCA. Even though D-OCA generally could show clearer choroidal vessels, some specific choroidal vessels are not visualized at all or are unclear, because the measurable flow velocity is limited. However, this limitation is counteracted in S-OCA because S-OCA is OCT intensity based method and is insensitive to phase.

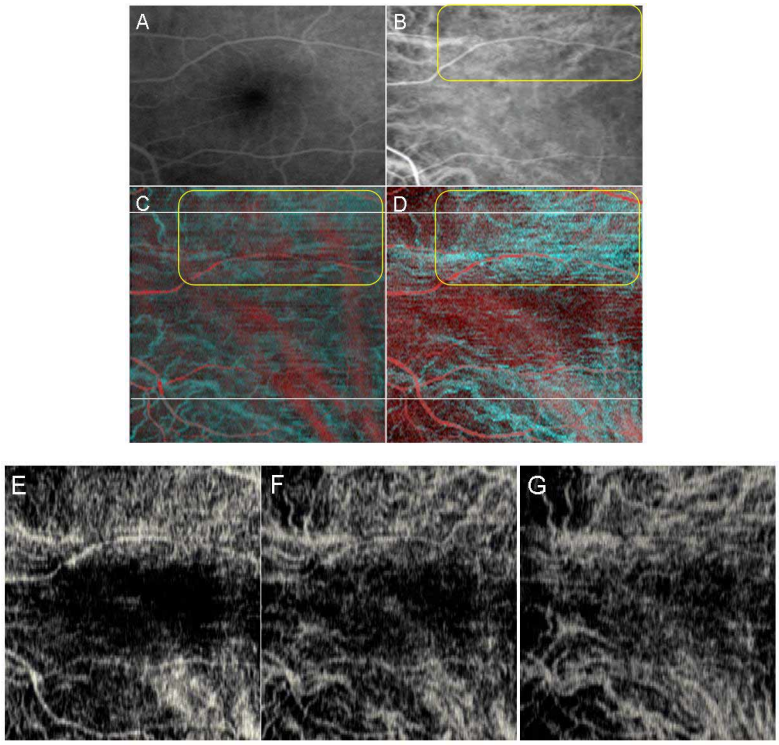

Fig. 6. Comparison of angiography images of the macula; each image is obtained using (A) FA, (B) ICGA, (C) D-OCA and (D) S-OCA. Subsections (E), (F) and (G) represent sliced images of the segmented choroidal vasculature at different depths relative to the RPE, i.e., at 71, 107, and 142 μm, respectively (2.45MB movie).

Figure 6 shows a comparison of the angiograms of the macula; Fig. 6(A): FA, Fig. 6(B): ICGA, Fig. 6(C): D-OCA, and Fig. 6(D): S-OCA. The S-OCA reveals a clearer image of the choroidal vasculature in the upper portion of the macular area, than that obtained using D-OCA, particularly in the yellow rectangular area. However, the fine choroidal vasculature that appears on the upper-right side of the macular area is not as clear as that shown in Fig. 6(C).

#80285 - $15.00 USD Received 22 Feb 2007; revised 2 May 2007; accepted 3 May 2007; published 5 Jun 2007

The integrating of these images respecting to the depth may have smeared the image of the fine structure of the vasculature. However, using the en face-sliced (C-scan) images of the segmented vasculature, we were able to distinguish the fine choroidal vasculature, as observed in Fig. 6(E), 6(F), and 6(G).

4.3 Comparison standard resolution S-OCA of and UHR S-OCA

The same subjects that were described in the sections 4.1 and 4.2 were measured using the UHR-SD-OCT system and the S-OCA algorithm was applied. Because the lateral resolution of the UHR-OCT is the same as that of the standard SD-OCT, the image performance of choroidal vessel segmentation is almost the same in the en-face plane. However, due to the high axial resolution, when we construct 3D choroidal vasculature, fine vessels are able to be segmented and we could produce the improved 3D image of the choroidal vasculature. Fig. 7(A) and 7(B) reveal the segmented choroidal vessels obtained using UHR-SD-OCT from macula and ONH, respectively. More choroidal vessels are visible and they are clealer than that of standard resolution S-OCA. Two 2D UHR-S-OCA aniograms of ONH and macula are attached together, as shown in Fig. 7(C). One noticeable this is that it is possible to recognize the horizontally stretched choroidal vessels more clearly in this figure than in Fig. 5(D) as indicated by the yellow arrows. It is also possible to find the connectivity of the vessels of two area, ONH and macula.

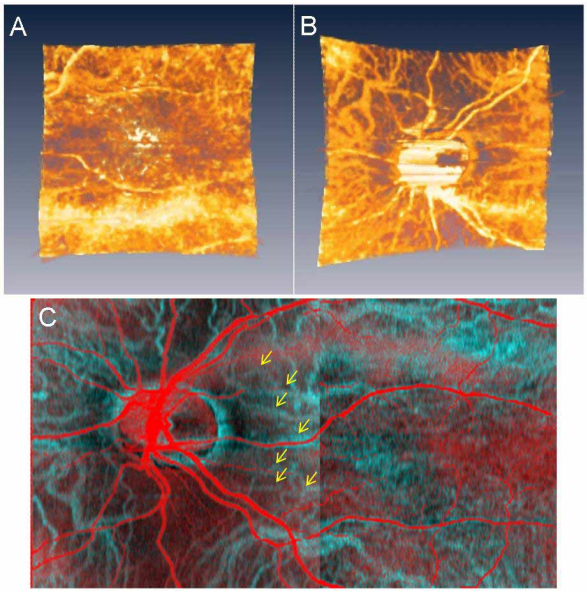

Fig. 7. 3D image of the choroidal vasculature obtained using the measurement results of UHR-SD-OCT with regard to (A) macula (1.93MB movie) and (B) ONH (1.91MB movie). (C) reveals an attached 2D S-OCA angiogram of ONH and macula

Figure 8 and Fig. 9 reveal the en-face slice images that were taken at every 14.5 μm relative to the RPE, in the macular and ONH areas, respectively. The segmented choriocapillaries beneath the RPE can be distinguished, and thicker choroidal vessels are visualized as the deeper regions are sliced.

#80285 - $15.00 USD Received 22 Feb 2007; revised 2 May 2007; accepted 3 May 2007; published 5 Jun 2007

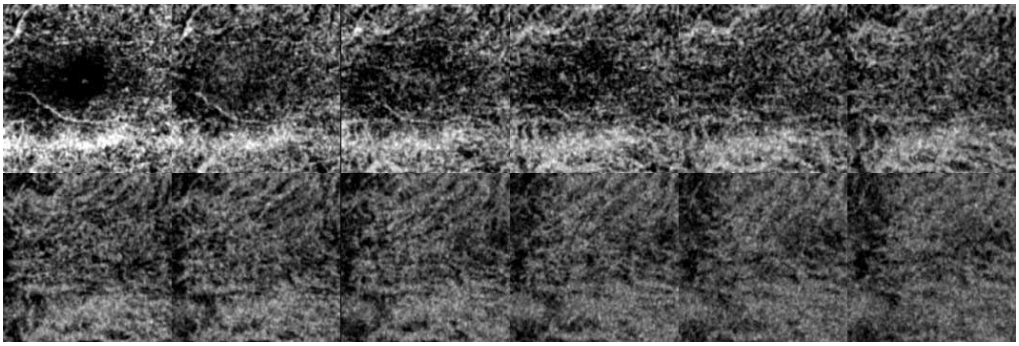

Fig. 8. En-face slice images of the macula are sliced every 14.5 μm relative to the RPE (2.49MB movie).

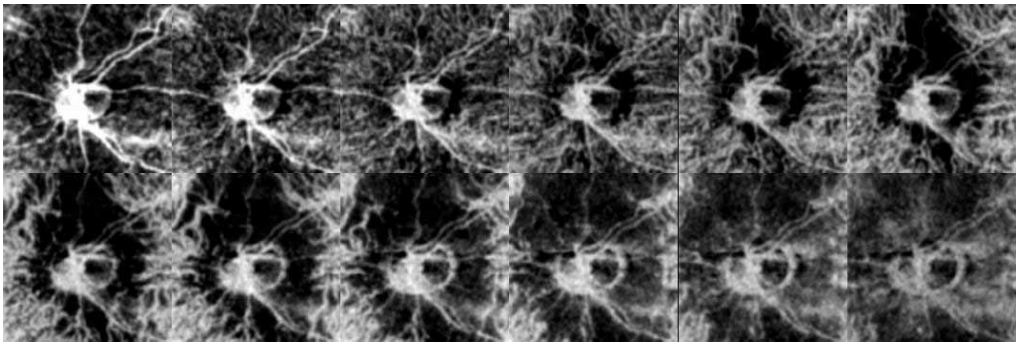

Fig. 9. En-face slice images of ONH are sliced every 14.5 μm relative to the RPE (2.47MB movie).

4.4 Comparison of S-OCA and simple inversion volume

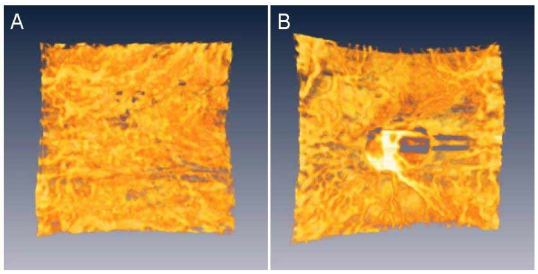

Fig. 10. Simple inversion of intensity volume of the (A) macula (1.98MB movie) and (B) ONH (1.95MB movie) processed using the UHR-SD-OCT results.

According to some point of view, the S-OCA algorithm appears identical to simple inversion of intensity volume, even though the algorithm contains several computations. In order to clearly demonstrate the advantage of the S-OCA, simply inverted intensity volume was created from the measurement results obtained using UHR-SD-OCT. As shown in Fig. 10, the simply inverted intensity volumes revealed the choroidal vessels; however, the clarity was not as good as that of S-OCA. For the identification of the choroids of the eye, we employed the segmentation of three layers; the anterior surface of the retina, the RPE complex and the virtual posterior boundary of the choroids. As mentioned in section 3, it is difficult to

#80285 - $15.00 USD Received 22 Feb 2007; revised 2 May 2007; accepted 3 May 2007; published 5 Jun 2007

ascertain the real position of the posterior boundary of the choroids; hence, we defined the posterior boundary as the greatest penetration depth, namely signal vanishing depth. This leads to the development of a low-signal region in the choroids. Because the low signal region that exists beneath the choroidal vessels is visualized with high intensity in the inverted intensity volume, the 3D image of the choroidal vasculature obtained by the simple inversion of intensity is not as good as that obtained using S-OCA. The advantage of the S-OCA method can be emphasized by the following explanation. The intensity decay was compensated by using a threshold that was obtained from each en-face plane. In addition, the segmentation process using the threshold based on the intensity distribution could eliminate the low signal region that exists under the choroidal vasculature.

4.5 S-OCA of the AMD

One of the advantages of the S-OCA method is that it reveals the choroidal vasculature with low-density scanning; this is because S-OCA functions based on the scattering property of blood and does not employ Doppler phase signal. That means measurement time could be reduced for the real patient, and it shows the feasibility of S-OCA. The macular area of an AMD patient was measured using our standard SD-OCT, and low-density OCT data (249 × 254 A-lines in 5 mm × 5 mm) were obtained in 3.3 s. As shown in Fig. 11(B), an S-OCA angiogram was then obtained. Some similarities were observed between S-OCA and ICGA. In the en-face-slice image of the segmented vessels shown in Figs. 11(C) and 11(D), the choroidal vasculature is resolved and appeares more clearer. One noticeable thing is the CNV lesion indicated with yellow closed circular arc in Fig. 11(A), we could find the similar pattern in the S-OCA angiograms as white region of Figs. 11(B) and 11(C).

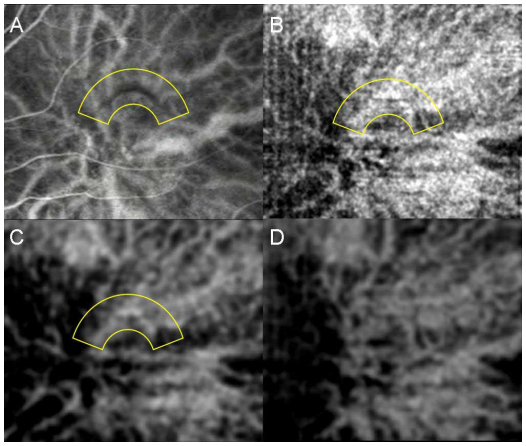

Fig. 11. Choroidal vascular images of the macula of an AMD patient were obtained using, (A) ICGA and (B) by projecting the segmented choroidal vessels. Subsections (C) and (D) are en-face slice images of the segmented vessels obtained at depths of 88.8 μm and 124.3 μm, respectively, from the RPE.

4.6 S-OCA of the polypoidal choroidal vasculopathy (PCV)

For the other application, the eye of the polypoidal choroidal vaculopathy (PCV) patient was measured by the standard SD-OCT. For this measurement, we employed high-density scanning of the 1024 and 140 A-lines in a 5 mm × 5 mm area. After the 3D reconstructing of the choroidal vasculature by using the S-OCA, some network structure was revealed beneath the pigment epithelial detachment (PED). Figure 12(A) and 12(B) show an image of the segmented choroidal vasculature, and combined image with the intensity structure of the retina, respectively. Figure 12(C) is the projection image of the segmented choroidal vessels. Figures 12(D), 12(E), and 12(F) are sliced images at the several different depths. Figures

#80285 - $15.00 USD Received 22 Feb 2007; revised 2 May 2007; accepted 3 May 2007; published 5 Jun 2007

12(G), 12(H), and 12(I) are zoom-in images of Fig. 12(D), 12(E) and 12(F), respectively, of the PED region. Some fine choroidal vessels are observed in the en-face slice images.

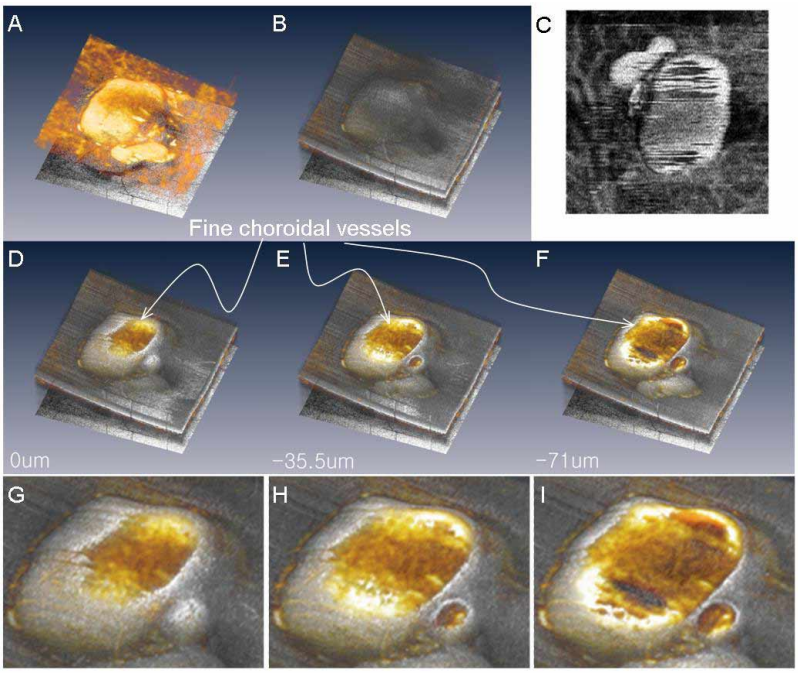

Fig. 12. (1.86MB movie) Fine choroidal vessels are visible beneath the epithelium in the ocular images of a PCV patient. (A) A 3D image of the segmented choroidal vasculature; (B) this image combined with an image of the structure of retinal volume; (C) projection image of the segmented choroidal vessels. (D), (E), and (F) reveal several slice images within the retinal volume and (G), (H), and (I) are zoom-in images of the PED region (4.89MB movie version).

#80285 - $15.00 USD Received 22 Feb 2007; revised 2 May 2007; accepted 3 May 2007; published 5 Jun 2007

5. Conclusions

S-OCA was applied to the 800 nm band SD-OCT. We obtained 2D projection images of the choroidal vessels and combined them with a retinal shadowgram. A comparison of this method with existing methods such as FA, ICGA, and D-OCA revealed some similarities in the image quality. We recommend and prefer the combined use of S-OCA and D-OCA method; this is because these methods have different contrast mechanism and complement each other in non-invasive angiography as discussed in section 4.2. We could resolve fine or faint vessels that are smeared in the 2D angiogram by using en-face slice image of the 3D vasculature. In addition, the application of S-OCA to UHR-SD-OCT measurement data produces improved 3D images of the choroidal vasculature. In order to test the clinical application of this method, two eyes of AMD and PCV are examined. Despite the use of low-density scan data, the 2D S-OCA of the AMD patient had an image quality similar to that of ICGA image. The fine chorodial vessels located beneath the PED were visualized in the PCV case by using high-density scan data. This method will prove to be more clinically relevant if the UHR-SD-OCT system is used with low-density scanning because this will reduce the measurement time and improve the visualization of choroidal vessels.

Acknowledgments

Youngjoo Hong is a guest student to the University of Tsukuba from Korea Advanced Institute of Science and Technology. Technical contributions from Yasuaki Hori have been gratefully acknowledged.

This research has been partially supported by a Grant-in-Aid for Scientific Research 18360029 from the Japan Society for the Promotion of Science (JSPS), Japan Science and Technology Agency, and the Special Research Project of Nanoscience at the University of Tsukuba.

Youngjoo Hong is partially supported by a Brain Korea 21 (BK21) and a scholarship from Youi-Giken, Shuichi Makita is supported by Japan Society for the Promotion of Science, and Masahiro Yamanari is partially supported by Japan Ministry of Education, Culture, Sports, Science and Technology through a contract under the Promotion of Creative Interdisciplinary Materials Science for Novel Functions, 21st Century Center of Excellence (COE) Program.

#80285 - $15.00 USD Received 22 Feb 2007; revised 2 May 2007; accepted 3 May 2007; published 5 Jun 2007